JACS
JOURNAL OF THE AMERICAN CHEMICAL SOCIETY
pubs.acs.org/JACS
Article

Network-Forming Liquids from Metal–Bis(acetamide) Frameworks with Low Melting Temperatures

Mengtan Liu, Ryan D. McGillicuddy, Hung Vuong, Songsheng Tao, Adam H. Slavney, Miguel I. Gonzalez, Simon J. L. Billinge, and Jarad A. Mason*

Cite This: https://dx.doi.org/10.1021/jacs.0c11718
Read Online
ACCESS | Metrics & More | Article Recommendations | Supporting Information

ABSTRACT: Molten phases of metal–organic networks offer exciting opportunities for using coordination chemistry principles to access liquids and glasses with unique and tunable structures and properties. Here, we discuss general thermodynamic strategies to provide an increased enthalpic and entropic driving force for reversible, low-temperature melting transitions in extended coordination solids and illustrate this approach through a systematic study of a series of bis(acetamide)-based networks with record-low melting temperatures. The low melting temperatures of these compounds are the result of weak coordination bonds, conformationally flexible bridging ligands, and weak electrostatic interactions between spatially separated cations and anions, which collectively reduce the enthalpy and increase the entropy of fusion. Through a combination of crystallography, spectroscopy, and calorimetry, enthalpic trends are found to be dictated by the strength of coordination bonds and hydrogen bonds within each compound, while entropic trends are strongly influenced by the degree to which residual motion and positional disorder are restricted in the crystalline state. Extended X-ray absorption fine structure (EXAFS) and pair distribution function (PDF) analysis of $Co(bba)_3[CoCl_4]$ [bba = *N*,*N*′-1,4-butylenebis(acetamide)], which features a record-low melting temperature for a three-dimensional metal–organic network of 124 °C, provide direct evidence of metal–ligand coordination in the liquid phase, as well as intermediate- and extended-range order that support its network-forming nature. In addition, rheological measurements are used to rationalize differences in glass-forming ability and relaxation dynamics. These results provide new insights into the structural and chemical factors that influence the thermodynamics of melting transitions of extended coordination solids, as well as the structure and properties of coordination network-forming liquids.

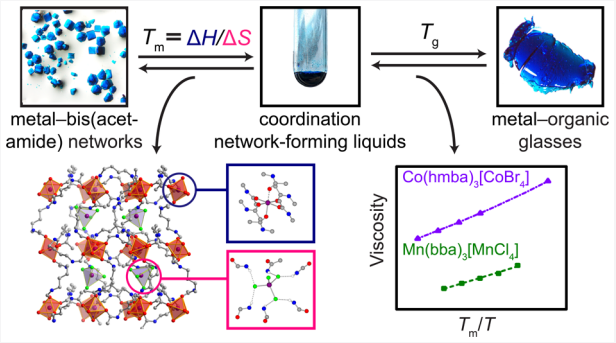

INTRODUCTION

Network-forming liquids feature extended structural correlations that influence many important macroscopic properties—including viscosity, conductivity, and density—and can lead to unique phase behavior.[1,2] In metal–organic framework chemistry, the extended structure—and free volume—of solids is routinely manipulated using coordination chemistry and reticular design principles to form networks of metals linked by bridging organic ligands.[3] Though in its infancy, the application of similar ideas to liquids offers exciting possibilities for expanding the structural and chemical diversity of network-forming liquids by providing access to new topologies and longer-range structural correlations mediated by the increased length of organic bridging ligands relative to the bridging atomic units of conventional network-forming materials such as SiO_2 and $ZnCl_2$.[4] However, even though tens of thousands of metal–organic networks have been reported in the literature,[5] there are surprisingly few examples of such compounds that have accessible and stable liquid states (Table S12).[4,6] Indeed, the limited examples of three-dimensional coordination networks that have been shown to melt into liquids are predominantly variants of zeolitic imidazolate frameworks (ZIFs).[4a,6a,c,d,e,j] Although ZIFs have provided an initial platform to begin exploring the structures and properties of liquid phases of metal–organic frameworks, their melting transitions typically occur at temperatures above 350–400 °C—often preceded by crystalline-to-amorphous transitions that make it challenging to establish relationships between structure and melting thermodynamics—and produce liquid phases that can be prone to decomposition. To realize the full potential of coordination network-forming liquids,[7] new strategies are needed to design metal–organic networks with lower melting temperatures that yield liquids with

Received: November 8, 2020

increased stability and a greater range of structures and compositions. Beyond harnessing the intrinsic chemical and physical properties of coordination network-forming liquids to establish new structure−property relationships and realize new functionalities, expanded access to molten phases of metal−organic frameworks would also afford new opportunities for materials processing,[8] growth of large single crystals,[9] and glass formation.[10]

The existence of matter in the liquid state requires that attractive interactions between constituent atoms, ions, molecules, or other chemical species are sufficiently counteracted by repulsive interactions—imparting fluidity while still maintaining cohesion. In principle, every metal−organic network has an equilibrium melting temperature, T_m. In practice, however, the decomposition temperature, T_{dec}, of many compounds falls below T_m. Therefore, the primary challenge in the synthesis of coordination network-forming liquids is to design systems for which $T_m < T_{dec}$.[6c] To date, the limited efforts to explore melting transitions in two- and three-dimensional metal−organic networks have focused on increasing T_{dec} through the use of ligands—such as imidazoles—with high thermal stabilities, while efforts to design compounds with intrinsically lower T_m have received comparatively little attention.[6c,e−g,j] Herein, we establish generalizable thermodynamic strategies to lower the melting temperature of three-dimensional metal−organic networks through the synthesis and characterization of a series of bis(acetamide)-based compounds that feature stable liquid phases (Figure 1).

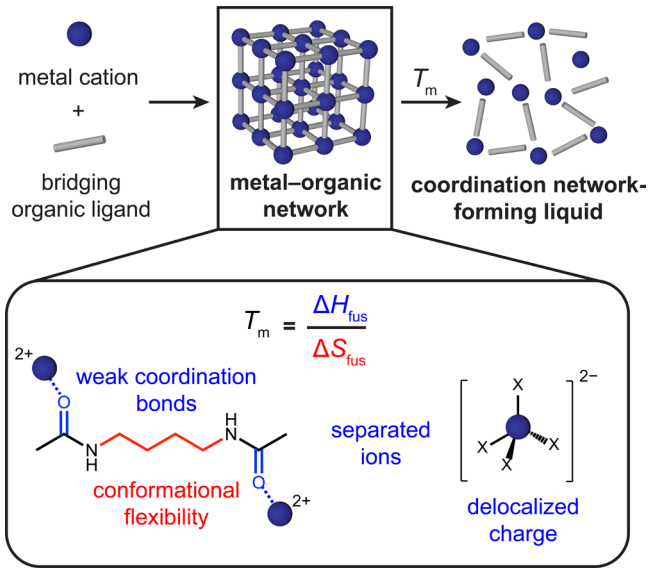

Figure 1. Illustration of design principles to promote the formation of coordination network-forming liquids from extended metal−organic materials by minimizing the enthalpy of fusion, ΔH_{fus}, and maximizing the entropy of fusion, ΔS_{fus}, to achieve low melting temperatures, T_m.

Our approach draws from the well-established "crystal engineering" design rules of metal−organic framework chemistry to control structure through directional coordination bonds and from the "anti-crystal engineering" design rules of ionic liquid synthesis to promote low melting temperatures.[3,6f,11] Specifically, we targeted organic ligands predisposed to (1) bridge multiple metals and (2) provide an enthalpic and entropic driving force for low-temperature melting transitions. Melting transitions are governed by the difference in enthalpy (ΔH_{fus}) and entropy (ΔS_{fus}) between solid and liquid phases, with the transition temperature given by $\Delta H_{fus} = T_m \Delta S_{fus}$. The promotion of low melting temperatures thus requires minimizing ΔH_{fus}, maximizing ΔS_{fus}, or some combination of both.

Minimizing ΔH_{fus} entails balancing the strength of cohesive interactions within the solid and liquid phases. In most metal−organic materials, such interactions involve a convolution of attractive and repulsive forces, including those mediated by coordination bonds, hydrogen bonds, van der Waal interactions, Coulombic interactions, and steric repulsions. For a three-dimensional metal−organic network to transition to a liquid, the network of coordination bonds holding the compound together must dissociate to at least some degree to enable the inherent microscopic fluctuations that give rise to the macroscopic fluidity of liquids. Indeed, simulations have indicated that tetrahedral Zn centers in Zn(imidazolate)$_2$ (ZIF-4) transition to an average coordination number of ∼3.3−3.6 in the liquid phase.[4a,c] Bridging ligands bearing coordination groups that form relatively weak bonds with metals—such as sulfonates, esters, amides, and nitriles—should facilitate the partial breaking of coordination bonds during melting and thus promote a lower enthalpy change—and lower melting temperature—than the carboxylate- and azolate-based ligands that are typically used to form metal−organic frameworks with high thermal stability.[6f,g,i,k] In addition, ΔH_{fus} can be further reduced by minimizing electrostatic attractions through charge delocalization and the spatial separation of anions and cations—a strategy that is routinely applied in the design of ionic liquids.[11]

Maximizing ΔS_{fus} requires minimizing solid-state entropy and maximizing liquid-state entropy. In most cases, the entropy of metal−organic materials can be partitioned into contributions from configurational, vibrational, and rotational entropy for solid phases, with an added contribution from translational entropy for liquid phases.[6e,f,12] Although much remains to be understood about relationships between the structure, composition, and entropy of metal−organic networks, their configurational, vibrational, and rotational entropy should, in principle, be conducive to predictable manipulation through ligand design. For instance, low-symmetry, high-flexibility organic bridging ligands will access more conformations in the liquid phase relative to the solid,[13] and consequently, compounds constructed from such ligands should experience a greater increase in entropy upon melting. Similarly, extended structures that better restrict the residual motion of organic ligands in the solid state should undergo higher entropy increases upon melting than structures for which ligands have more rotational and vibrational degrees of freedom in the solid state.

Toward the goal of minimizing ΔH_{fus} and maximizing ΔS_{fus}, we targeted extended networks composed of flexible bridging ligands with weak, neutral donor groups and noncoordinating anions to provide charge balance (Figure 1). Although there are limited examples of three-dimensional coordination networks formed exclusively from neutral bridging ligands, select polymethylene bis(amides) are known to form crystalline two- and three-dimensional extended solids with several first-row transition metals (Table S13),[14] a few of which even have reported visual melting points.[14b] We hypothesized that metal−amide bonds would provide an interaction weak enough to facilitate melting, but strong

https://dx.doi.org/10.1021/jacs.0c11718
J. Am. Chem. Soc. XXXX, XXX, XXX−XXX

enough to dictate the orientation and arrangement of bridging ligands through directional interactions.[15] As such, we anticipated that bis(amide)-based coordination networks would provide a highly tunable platform to access metal–organic networks with low melting temperatures and to explore the thermodynamics, structures, and properties of new classes of network–forming liquids.

RESULTS AND DISCUSSION

Thermal Characterization of Three-Dimensional Metal–Bis(acetamide) Networks. To begin investigating melting phenomena in metal–bis(amide) networks, we synthesized the compound $Co(hmba)_3[Co(NCS)_4]$ [hmba = *N*,*N*′-1,6-hexamethylenebis(acetamide)] and characterized its thermal behavior by differential scanning calorimetry (DSC). In this crystalline extended solid, octahedral Co centers are bridged through the carbonyl O atoms of hmba ligands—with two pairs of equatorial ligands connecting to two neighboring Co centers to form chains that are further connected by axial hmba ligands—to yield a three-dimensional, cationic network.[14b] Charge balance is provided by $[Co(NCS)_4]^{2-}$ anions that fill the network voids (Figure S8). Excitingly, DSC revealed a fully reversible melting transition at 144 °C with a ΔH_{fus} of 108 kJ/mol (Figure 2). While thermal decomposition,

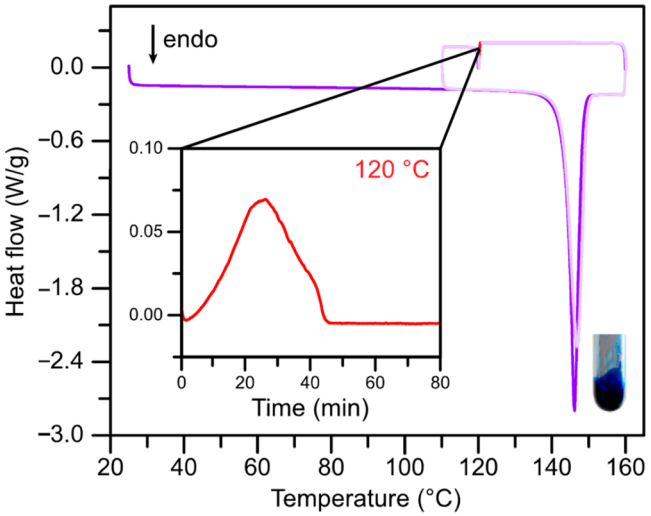

Figure 2. Differential scanning calorimetry (DSC) traces for $Co(hmba)_3[Co(NCS)_4]$ with heating and cooling rates of 5 °C/min. The dark purple trace corresponds to the first heating–cooling cycle, while the two overlapping light purple traces correspond to subsequent cycles under the same conditions. An image of the liquid phase inside a glass tube is shown at the bottom right. Inset: An isothermal hold at 120 °C led to complete recrystallization.

phase separation, large changes in porosity, or high viscosity preclude recrystallization for all molten three-dimensional metal–organic networks reported to date,[6a,c,d,f] $Co(hmba)_3[Co(NCS)_4]$ features high thermal stability in the liquid state (Figure S23) and can be fully recrystallized upon holding the supercooled melt at 120 °C for less than 1 h (Figure 2).

The low melting temperature of $Co(hmba)_3[Co(NCS)_4]$ can be attributed, in part, to a large ΔS_{fus} of 260 J/mol·K. In addition to contributions from an anticipated decrease in the average coordination number of network Co atoms, this large entropy change during melting likely arises from the high conformational flexibility of hmba and the increased rotation and mobility of uncoordinated anions in the liquid phase. To better understand the relative contributions of different structural and chemical factors to melting thermodynamics, we endeavored to synthesize and compare the thermal behavior of a series of metal–organic networks with the same coordination bonding motifs but different metals, bridging organic ligands, and uncoordinated anions. Because of the limited variability and large size of $[M(NCS)_4]^{2-}$ anions, we specifically targeted compounds with similar topologies but more compact and tunable $[MX_4]^{2-}$ (X = Cl, Br) anions.

Although combining metal halides with hmba tends to yield two-dimensional networks,[14a] we found that shorter bis(acetamide) ligands, which template smaller voids that better accommodate $[MX_4]^{2-}$ anions, promote the formation of three-dimensional structures. Specifically, combining *N*,*N*′-1,4-butylenebis(acetamide) (bba) with divalent metal chloride salts led to the new series of three-dimensional networks $M(bba)_3[M'Cl_4]$ (M/M′ = Mn, Fe, Co; M = Mn, M′ = Zn; and M = Mg, M′ = Co, Zn). Single-crystal X-ray diffraction (SCXRD) revealed that all compounds crystallize in the same space group ($Pa\bar{3}$) with the same three-dimensional connectivity, wherein octahedral metal centers are each connected to six other metal centers by bridging bba ligands to form a three-dimensional cubic network that surrounds tetrahedral uncoordinated anions (Figure 3a). Moreover, all six compounds undergo reversible melting transitions that span from 124 °C for $Co(bba)_3[CoCl_4]$ to 262 °C for $Mg(bba)_3[ZnCl_4]$ (Figure 3c, Figure S19). To the best of our knowledge, the melting temperature of $Co(bba)_3[CoCl_4]$ is the lowest yet reported for a three-dimensional coordination network (Table S12).

Prior to melting, TGA with a temperature ramp rate of 2 °C/min indicates minimal mass loss (<1.5 wt %) for all compounds that have melting temperatures below 200 °C (Figures S28 and S31). With a melting temperature of 260 °C, the larger mass loss of $Mg(bba)_3[CoCl_4]$ prior to melting (17% at 2 °C/min and 7% at 10 °C/min, Figure S29)—as well as mass loss from the liquid state of other compounds—is attributed to volatilization of the neutral bridging ligand under flowing N_2 gas. Despite their volatility in an open system, the liquid phases of each compound exhibit high thermal stability in a closed system as evidenced by DSC cycling experiments (Figures S19, S30, and S31).

Trends in Melting Thermodynamics. The $M(bba)_3[M'Cl_4]$ series of compounds illustrate how structure impacts the interplay between enthalpy and entropy that ultimately dictates the melting temperature of metal–organic networks. Within this series, $Co(bba)_3[CoCl_4]$ has the lowest melting temperature of 124 °C, while $Mn(bba)_3[MnCl_4]$ and $Mg(bba)_3[CoCl_4]$ have much higher melting temperatures of 172 and 260 °C, respectively. As evidenced by the nearly identical melting temperatures of $Mg(bba)_3[CoCl_4]$ and $Mg(bba)_3[ZnCl_4]$ (Figure S19), differences in melting behavior seem to be governed primarily by network metal atoms, while the identity of the metal in the charge-balancing anion has minimal influence. This is confirmed by variable temperature extended X-ray absorption fine structure (EXAFS) spectra of $Mg(bba)_3[CoCl_4]$ at the Co K edge, which show minimal structural changes to $[CoCl_4]^{2-}$ anions upon melting (Figure S33).

Surprisingly, the driving force for the higher melting temperature of $Mn(bba)_3[MnCl_4]$ relative to the Co and Fe

https://dx.doi.org/10.1021/jacs.0c11718
J. Am. Chem. Soc. XXXX, XXX, XXX–XXX

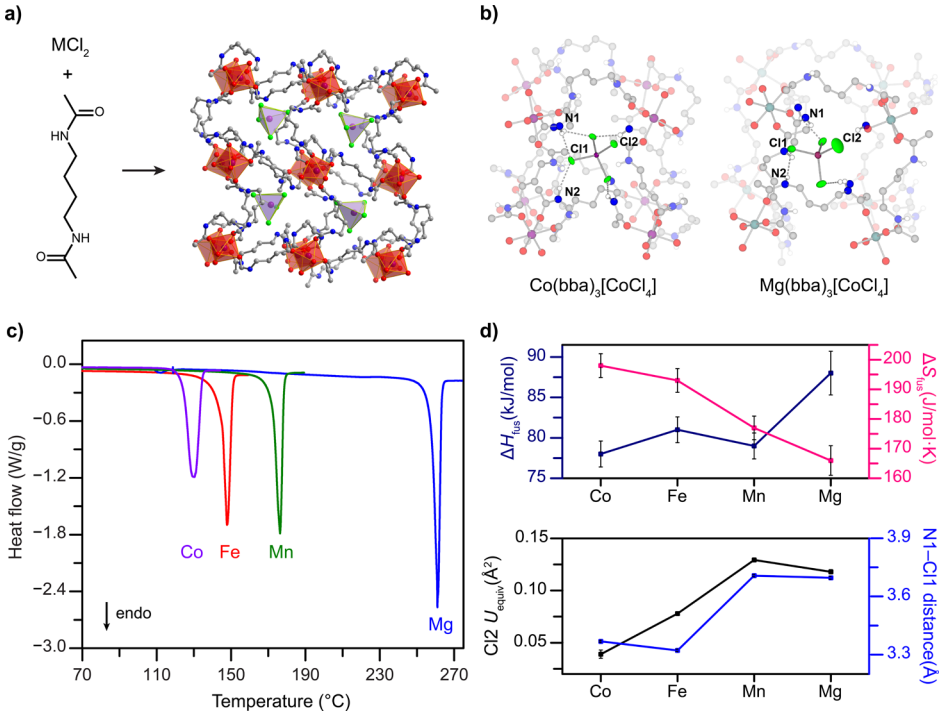

Figure 3. (a) Crystal structure of the three-dimensional network $Co(bba)_3[CoCl_4]$. Note that the bba ligand is disordered over two positions, and only the higher occupancy atomic positions are shown. Purple, red, gray, blue, and green spheres represent Co, O, C, N, and Cl atoms, respectively; H atoms have been omitted for clarity. (b) The geometry of hydrogens bonds to $[CoCl_4]^{2-}$ anions is compared for $Co(bba)_3[CoCl_4]$ and $Mg(bba)_3[CoCl_4]$ at 100 K to highlight the additional set of moderate hydrogen-bonding interactions present in the former compound. Atomic displacement parameters are shown at 50% probability for $[CoCl_4]^{2-}$ counteranions. Teal spheres represent Mg atoms, and only N−H protons are shown. For $Co(bba)_3[CoCl_4]$, note that the lower occupancy position of the bba ligand is shown as this has slightly shorter hydrogen bond distances. (c) DSC traces for $M(bba)_3[M'Cl_4]$ compounds (M/M′ = Co, Fe, Mn; and M = Mg, M′ = Co) with a heating rate of 5 °C/min for all compounds. (d) Top: Trends in ΔH_{fus} and ΔS_{fus} are illustrated for $Co(bba)_3[CoCl_4]$, $Fe(bba)_3[FeCl_4]$, $Mn(bba)_3[MnCl_4]$, and $Mg(bba)_3[CoCl_4]$. Error bars reflect a 2% instrumental error. Bottom: The equivalent isotropic displacement parameters, U_{equiv}, of Cl2 atoms and the N1−Cl1 hydrogen bond donor−acceptor distances at 100 K are generally correlated to one another and inversely correlated to ΔS_{fus}. Note that donor−acceptor distances were weighted by relative occupancy to account for two-part disorder when present.

analogues is primarily entropic in nature, while that for the Mg analogue is both enthalpic and entropic. More specifically, the higher melting temperature of $Mn(bba)_3[MnCl_4]$, which has a similar ΔH_{fus} to the Co and Fe analogues, is the result of a lower ΔS_{fus}, while the even higher T_m of the Mg analogue is due to both a lower ΔS_{fus} and higher ΔH_{fus} (Figure 3d). These thermodynamic differences reveal an absence of enthalpy−entropy compensation—where changes to ΔH are offset by proportionate changes to ΔS—and indicate that independent molecular mechanisms contribute to the enthalpy and entropy of fusion in this system.[13b,16]

Enthalpic trends can be rationalized, at least in part, on the basis of M−O coordination bond strength, which is expected to follow the trend Mn−O < Fe−O < Co−O < Mg−O.[17] Stronger Mg−O bonds likely lead to the larger ΔH_{fus} of $Mg(bba)_3[CoCl_4]$ through two mechanisms: (1) more energy will be required to partially break Mg−bba bonds and reduce the average metal coordination number during melting and (2) more energy will be required to partially break hydrogen bonds between amides and uncoordinated anions when the amide carbonyl is more polarized through a stronger interaction with Mg centers. The similar ΔH_{fus} of the Mn, Fe, and Co analogues can be attributed to small differences in metal−ligand bond strength that may be offset by differences in the hydrogen bond acceptor strength of $[MCl_4]^{2-}$ anions or by slight differences in the average metal coordination number after melting.[18]

Unlike ΔH_{fus}, M−O bond strength does not have a clear influence on entropic trends within this series of compounds. Specifically, while $Co(bba)_3[CoCl_4]$ and $Fe(bba)_3[FeCl_4]$ should have M−O bonds of intermediate strength,[17] their entropy changes are considerably higher than both the Mn and Mg analogues. Explaining this surprising result in a manner that is consistent with trends in enthalpy is not trivial, as most molecular mechanisms would predict at least some degree of enthalpy−entropy compensation. That is, the breaking of stronger interactions would typically lead to larger increases in both enthalpy and entropy of fusion within a given system.[19] In this case, the high ΔS_{fus} of the Co and Fe analogues—and, consequently, their low melting temperatures—can be rationalized, at least in part, through subtle structural differences between these compounds and their Mg and Mn congeners. Although each network crystallizes with the same three-dimensional connectivity and local coordination environment around metal centers, a ∼170° difference in the N1−C3−C4−C5 dihedral angle of bba bridging ligands in $Co(bba)_3[CoCl_4]$ and $Fe(bba)_3[FeCl_4]$ relative to the Mg and Mn analogues leads to a different arrangement of hydrogen bonds between the N−H protons of bba and the Cl atoms of uncoordinated anions (Figure S3). Specifically, each network contains two crystallographically independent Cl sites, with each $[MCl_4]^{2-}$ anion centered on a 3-fold rotation axis that lead to three Cl1 atoms and one Cl2 atom (Figure 3b). In $Fe(bba)_3[FeCl_4]$ and $Co(bba)_3[CoCl_4]$, each Cl1 is

https://dx.doi.org/10.1021/jacs.0c11718
J. Am. Chem. Soc. XXXX, XXX, XXX−XXX

engaged in two hydrogen-bonding interactions of moderate strength with donor–acceptor distances of less than 3.5 Å and bond angles greater than 120°.[20] In contrast, each Cl1 in the Mg and Mn analogues forms one moderate hydrogen bond (3.3 Å donor–acceptor distance) and one very weak hydrogen bond (≥3.7 Å donor–acceptor distance) (Table S7). This is corroborated by IR data, where the N–H stretch (~3290 cm^{-1}) of $Co(bba)_3[CoCl_4]$ and $Fe(bba)_3[FeCl_4]$ are both red-shifted by ~5 cm^{-1} compared to $Mg(bba)_3[CoCl_4]$ and $Mn(bba)_3[MnCl_4]$ (Figure S47).

We hypothesized that the additional set of moderate hydrogen bonds to Cl1 atoms in Co and Fe analogues reduces the entropy of the solid phase—and thus increases the entropy change upon melting—through two primary effects: (1) decreased residual motion of the counteranions and ligands, which reduces vibrational and rotational entropy, and (2) less disorder in the equilibrium positions of counteranion atoms, which reduces configurational entropy.[12,21] Since the equivalent isotropic atomic displacement parameters (U_{equiv}) obtained from crystal structure refinement describe the deviation of an atom's electron density from its average position, accounting for both local motion of atoms (dynamic disorder) and small deviations in their equilibrium positions (static disorder),[22] we anticipated that U_{equiv} might serve as an indicator of the relative entropy of the anions within each compound. Indeed, we found that U_{equiv} values for Cl2 atoms, which do not directly engage in moderate-strength hydrogen bonding interactions and thus have greater inherent mobility, were substantially lower in compounds with higher ΔS_{fus} (Figure 3d). Specifically, U_{equiv} at both 100 and 298 K is lower for Cl2 in $Co(bba)_3[CoCl_4]$ and $Fe(bba)_3[FeCl_4]$, which have higher ΔS_{fus}, than in the Mn and Mg analogues, which have lower ΔS_{fus} (Figure 3d, Figure S6). Assuming that all $[MCl_4]^{2-}$ anions have similar rotational, vibrational, and translational degrees of freedom in the liquid state, this offers a compelling potential explanation for the high ΔS_{fus} of the Co and Fe analogues, whereby the lower solid-state entropy conferred by more constrained $[MCl_4]^{2-}$ anions drives a larger entropy increase upon conversion to a liquid. Although the density and strength of hydrogen bonds to $[MCl_4]^{2-}$ anions could impact ΔH_{fus} in addition to ΔS_{fus}, the weak nature of these interactions likely reduces the magnitude of enthalpic effects arising from differences in hydrogen bonds relative to differences in coordination bonds, particularly if hydrogen bonds to $[MCl_4]^{2-}$ anions are largely preserved in the melt.

In addition to the residual motion and positional disorder of the $[MCl_4]^{2-}$ anions, other factors may contribute to the lack of enthalpy–entropy compensation—and, consequently, the large range of melting temperatures—exhibited by the $M(bba)_3[M'Cl_4]$ series of compounds. The high T_m of $Mg(bba)_3[CoCl_4]$, for instance, is the result of this compound having both the highest ΔH_{fus} and lowest ΔS_{fus} of the series. The high ΔH_{fus} can be attributed to stronger Mg–O bonds, which need to be at least partially broken in order for melting to occur. These stronger bonds also appear to restrict the residual motion of the bba ligand to a greater extent at 298 K than in other analogues as evidenced by the smaller average thermal displacement parameters for the bba ligand atoms of $Mg(bba)_3[CoCl_4]$ (Figure S7). This does not, however, provide a large enough entropic effect to compensate for the higher ΔH_{fus}, likely because differences in the residual motion of bba ligands are relatively small and decrease with increasing temperature.

Two-Dimensional Metal–Bis(acetamide) Networks. Beyond metal cation identity, the incorporation of different anions into metal–bis(acetamide) networks offers additional insight into the structural and chemical factors that contribute to their melting thermodynamics. For instance, combining $MgCl_2$ with bba under suitable conditions affords the compound $Mg(bba)_3Cl_2$, which has uncoordinated Cl^- instead of $[MCl_4]^{2-}$ anions and adopts a two-dimensional hexagonal network with Mg centers in a similar coordination environment as in the three-dimensional $Mg(bba)_3[CoCl_4]$ (Figure 4). Notably, this compound has a 70% higher ΔH_{fus} relative to

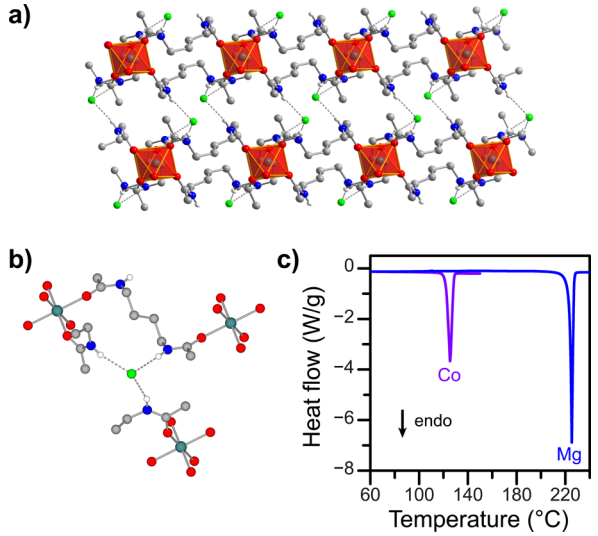

Figure 4. Crystal structure of $Mg(bba)_3Cl_2$ highlighting the (a) two-dimensional coordination network and (b) hydrogen bonds to Cl^- anions (dashed lines). Teal, red, gray, blue, green, and white spheres represent Mg, O, C, N, Cl, and H atoms, respectively. Only N–H protons are shown for clarity. (c) DSC traces for $Mg(bba)_3Cl_2$ (blue) and $Co(bba)_3Br_2$ (purple) with a heating rate of 5 °C/min.

$Mg(bba)_3[CoCl_4]$, increasing from 88 to 141 kJ/mol (Figure 5). This increase can be explained by stronger hydrogen bonds

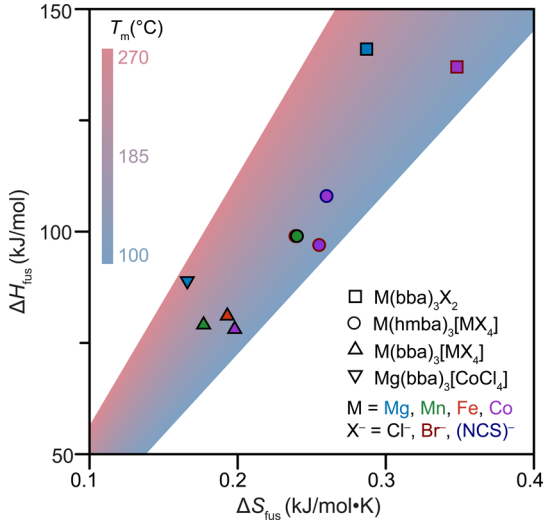

Figure 5. Comparison of ΔH_{fus}, ΔS_{fus}, and T_m for select metal–bis(acetamide) frameworks. The symbol shape identifies the series of compounds, while the symbol color designates the metal, and the border color designates the anion.

https://dx.doi.org/10.1021/jacs.0c11718
J. Am. Chem. Soc. XXXX, XXX, XXX–XXX

between bba ligands and the more charge-dense Cl^-acceptors. Despite this much larger enthalpy change, the melting temperature of $Mg(bba)_3Cl_2$ is actually 40 °C below that of $Mg(bba)_3[CoCl_4]$ (Figure 4c), indicating that, unlike within the $M(bba)_3[M'Cl_4]$ compounds, the increase in ΔH_{fus} is fully compensated for by an increase in ΔS_{fus} (Figure 5).

The large increase in entropy upon melting for $Mg(bba)_3Cl_2$ can be at least partially attributed to reduced entropy in the solid phase, as strong hydrogen bonds restrict the conformational flexibility of bba bridging ligands and reduce their residual motion and positional disorder within the crystal to a greater extent than strong M−O bonds. Indeed, while the bba ligand is disordered over two positions in $M(bba)_3[M'Cl_4]$, there is no disorder in the crystal structure of $Mg(bba)_3Cl_2$. In addition, U_{equiv} values for the O, C, and N atoms of bba ligands engaged in hydrogen bonds to Cl anions decrease by more than 40% compared to those of ligands hydrogen bonded to $[MX_4]^{2-}$ anions, which is consistent with reduced residual motion and positional disorder in the presence of stronger hydrogen bonds (Figure S7). The compound $Co(bba)_3Br_2$, which adopts a similar two-dimensional structure,[14a] also experiences an increase in ΔH_{fus} and ΔS_{fus} along with lower U_{equiv} values. Unlike the reversible melting transition of $Mg(bba)_3Cl_2$, however, $Co(bba)_3Br_2$ melts irreversibly. Variable temperature EXAFS spectra (Figure S33) reveal that this irreversibility is due to Br^- anions binding to Co centers in the liquid phase after melting, and powder X-ray diffraction suggests the partial formation of a new phase upon cooling, which appears to adopt the same network structure as $Co(bba)_3[CoCl_4]$ (Figure S13).

In addition to reducing solid-state entropy by restricting residual motion, halide anions should also affect the liquid-state entropy of $Mg(bba)_3Cl_2$ differently from tetrahalometallate anions. Specifically, while the lower rotational symmetry of tetrahalometallate anions will lead to a larger increase in rotational entropy upon melting, this is estimated to contribute just 6 J/mol·K to the overall entropy change.[13a,23] On the other hand, the smaller size of halide anions should result in greater mobility in the liquid phase and a larger increase in translational entropy upon melting,[24] which will be amplified by the fact that there are twice as many halide anions present as tetrahalometallate anions. The combination of restricted residual motion of bba in the solid state and increased translational entropy of halide anions in the liquid state—tempered by the slight decrease in rotational entropy in the liquid from the higher symmetry anion—can explain the increased ΔS_{fus} of $Mg(bba)_3Cl_2$ relative to $Mg(bba)_3[CoCl_4]$.

While the thermodynamic implications of the different liquid structure of $Co(bba)_3Br_2$ requires further study, the entropic impact of the restricted residual motion of bba bridging ligands in the two-dimensional $M(bba)_3X_2$ compounds highlights an opportunity for expanding the diversity of metal−organic networks with accessible melting transitions. Specifically, porosity can impart organic ligands with a high degree of residual motion in the solid state,[25] which raises the entropy of the solid and, consequently, reduces the entropy increase upon melting. We speculate that this may be, in part, why many metal−organic compounds have high melting points that exceed thermal decomposition temperatures, which would be consistent with a recent study reporting a decrease in the solid−liquid transition temperature of amorphous ZIF-62 with increasing pressure.[6h] As such, strategies to restrict the solid-state motion of organic bridging ligands, without compromising porosity, might provide an unexplored pathway to lowering the melting temperature of metal−organic frameworks.

Network-Forming Nature of the Liquid State. To probe the local structure of the liquid phase of metal−bis(acetamide) networks and to determine if any intermediate- or extended-range order is present, we collected variable-temperature X-ray total scattering data for $Co(bba)_3[CoCl_4]$ (Figure S36). The raw data images were integrated, corrected for experimental effects, and normalized using PDFgetX3 to obtain total scattering reduced structure functions, $F(Q)$, (Figure S37), which were Fourier transformed to obtain pair distribution functions (PDFs), $G(r)$ (Figure 6).[26] At short

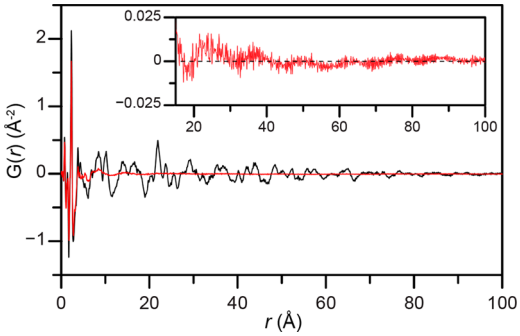

Figure 6. Pair distribution functions of $Co(bba)_3[CoCl_4]$ in the crystalline solid phase just below the melting temperature (black) and in the liquid phase above the melting temperature (red). Quasiperiodic oscillations indicative of extended-range order are shown in the inset.

scattering distances ($0 < r < 4$ Å), the liquid-phase PDF remains largely unchanged from the crystalline phase, with sharp features that can be assigned to C−C, C−N, and C−O bonds within the bba ligands, Co−Cl bonds of the $[CoCl_4]^{2-}$ anions, and Co−O bonds of the coordination network (Figures S42 and S43). This suggests that the average local coordination environment around Co centers is not substantially altered after melting.

Coordination of bba ligands in the melt was further confirmed by variable temperature EXAFS spectra, which can be well modeled with half of the Co centers in the melt coordinated to 4 Cl atoms—consistent with the persistence of $[CoCl_4]^{2-}$ anions in the melt—and half of the Co centers coordinated to 4.8(7) O atoms of bba ligands (Figure S35). The decrease in the coordination number of the network Co centers by 1.2 (20%) upon melting is consistent with molecular dynamics studies for ZIF-4 that suggest a decrease in coordination number upon melting from 4 to 3.3 (18%) or 3.6 (10%)[4a,c] and is distinct from the ionic liquid-like molten state of zinc−phosphate−azole coordination polymers, wherein ligand coordination to Zn is not preserved upon melting.[6b] Moreover, the average coordination number of 4.8(7) is well above the bond percolation threshold of 2.4 for a three-dimensional aperiodic network,[27] which indicates that, in spite of its dynamic nature, coordination between Co centers and bridging bba ligands in the melt is persistent enough for there to be pathways of extended connectivity that span the entire liquid.

Beyond the local coordination environment, the PDF of molten $Co(bba)_3[CoCl_4]$ exhibits peak broadening and decreased peak intensities that are consistent with the formation of a liquid phase with no long-range periodicity

https://dx.doi.org/10.1021/jacs.0c11718
J. Am. Chem. Soc. XXXX, XXX, XXX−XXX

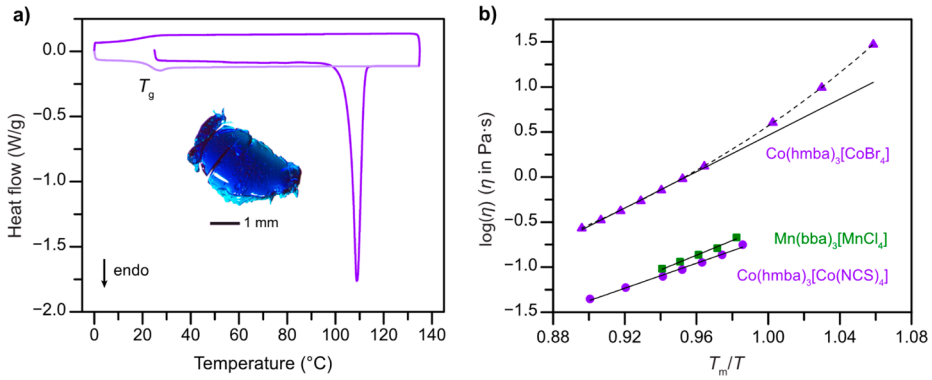

Figure 7. (a) DSC trace for Co(hmba)$_3$[CoBr$_4$] with heating and cooling rates of 5 °C/min. A glass transition is observed at 23 °C during the second heating run (light purple trace), which leads to the formation of a homogeneous, continuous glass film. (b) Temperature-dependent viscosity measurements of Co(hmba)$_3$[CoBr$_4$], Mn(bba)$_3$[MnCl$_4$], and Co(hmba)$_3$[Co(NCS)$_4$] are shown as purple triangles, green squares, and purple circles, respectively. The measurement temperatures are normalized to each respective melting temperature. The dashed black line represents a VFT fit for Co(hmba)$_3$[CoBr$_4$], while solid black lines represent Arrhenius fits.

and substantially less intermediate-range order than the crystalline solid phase. However, further PDF analysis reveals intermediate- and extended-range order that resembles the underlying network structure of the parent crystalline phase, as is characteristic of conventional network-forming liquids. Specifically, a first sharp diffraction peak (FSDP), which is a common feature of network-forming liquids and glasses, is observed in the total scattering reduced structure function, $F(Q)$, at 0.98 Å^{-1} (Figure S37). Though broadened and weaker in intensity, the FSDP for the liquid phase is only shifted slightly with respect to the FSDP of 0.91 Å^{-1} for the high-temperature crystalline solid phase, which suggests a small contraction upon melting and the persistence of some degree of intermediate-range order. Moreover, broad peaks centered at r = 8.4 and 14.3 Å in the liquid PDF represent intermediate-range structural correlations over length scales that are similar to the nearest-neighbor and second-nearest-neighbor Co−Co distances in the crystalline solid (Figure S40, Table S25).

Importantly, close examination of the high-r region reveals quasiperiodic oscillations that persist to at least 80 Å in the liquid (Figure 6, inset). These oscillations indicate the presence of extended-range structural correlations that exceed the common correlation length scale of charge ordering in ionic liquids and molten salts,[28] and resemble the density fluctuations that arise from topological and chemical ordering in network-forming liquid and glassy materials such as a-Si and $ZnCl_2$.[2f,29] While quasiperiodic oscillations have been observed in many metal−organic glasses up to at least 30 Å, and may be obscured at higher r by low signal to noise,[6b,j,30] this represents, to the best of our knowledge, the first observation of extended-range order in a metal−organic liquid. We anticipate that bridging ligand coordination and extended-range structural correlations will also occur in the liquid phases of other reversibly melting metal−bis(acetamide) networks, but additional characterization is necessary to confirm this.

Recrystallization Kinetics and Glass Formation. To further investigate the properties of liquid phases of metal−bis(acetamide) networks, we evaluated their behavior upon cooling through DSC experiments and variable temperature viscosity measurements. Although melting transitions are fully reversible for all but two compounds, liquid recrystallization kinetics vary dramatically during cooling, ranging from rapid crystallization to easily accessible glass transitions. For instance, when cooled at 10 °C/min from 20 °C above their melting temperature, three representative compounds—Mn(bba)$_3$[MnCl$_4$], Co(hmba)$_3$[Co(NCS)$_4$], and Co(hmba)$_3$[CoBr$_4$]—undergo rapid recrystallization, slow recrystallization, and a glass transition, respectively. More specifically, molten Mn(bba)$_3$[MnCl$_4$] fully recrystallizes even when cooled at high rates of 40 °C/min, while Co(hmba)$_3$[Co(NCS)$_4$] only completely recrystallizes during cooling when held 20 °C below T_m for 30−60 min and otherwise undergoes a glass transition. In contrast, Co(hmba)$_3$[CoBr$_4$] does not recrystallize under any conditions evaluated here—including after days at ambient temperature—and a homogeneous, transparent glass film is formed upon cooling, with a glass transition temperature, T_g, of 23 °C (Figure 7a). The larger T_g/T_m ratio of Co(hmba)$_3$[CoBr$_4$] (T_g/T_m = 0.78) relative to Co(hmba)$_3$[Co(NCS)$_4$] (T_g/T_m = 0.70) is consistent with the higher glass-forming ability of the former compound, while all other liquid phases with measurable T_g in this study have T_g/T_m ratios in between these values, which are slightly higher than the commonly observed 2/3 ratio (Table S15).[31]

To better understand the different recrystallization kinetics and glass-forming ability of these three metal−bis(acetamide) liquids, we compared their viscosities just above their melting temperatures. While all three liquids have comparable or higher viscosity to many glass-forming ionic liquids (Table S28), the viscosity of Co(hmba)$_3$[CoBr$_4$] is nearly an order of magnitude higher than that of the other two liquids (Figure 7b). This higher viscosity leads to slower relaxation dynamics that, in combination with the smaller amount of thermal energy available for nucleation at its lower melting temperature, could explain why Co(hmba)$_3$[CoBr$_4$] is the best glass former.[32] Since molten Mn(bba)$_3$[MnCl$_4$] and Co(hmba)$_3$[Co(NCS)$_4$] have very similar viscosities near their respective melting temperatures, the faster recrystallization kinetics of the former compound is likely the result of its higher T_m making activation energy barriers for nucleation easier to overcome because of increased thermal energy.

Further analysis of the temperature dependence of viscosity provides additional insight into liquid dynamics. Just above their respective melting temperatures ($0.9 < T_m/T < 1$), the viscosity of each melt appears to follow Arrhenius behavior as described by

https://dx.doi.org/10.1021/jacs.0c11718
J. Am. Chem. Soc. XXXX, XXX, XXX−XXX

$$\eta(T) = A \exp\left(\frac{E_a}{RT}\right)$$

where A is a temperature-independent constant and E_a is the activation energy of viscous flow (the energy barrier each component of the liquid needs to overcome to diffuse pass one another).[33] However, this Arrhenius dependence becomes nonphysical when extrapolated over a broader temperature range, significantly underestimating viscosities at both high and low temperature limits (infinite temperature and near T_g, respectively; Figure S45). This indicates E_a varies with temperature, which could be associated with structural heterogeneity and nonlinearity in relaxation dynamics.[34] Though recrystallization of $Mn(bba)_3[MnCl_4]$ and $Co(hmba)_3[Co(NCS)_4]$ occurs too quickly below T_m to allow for viscosity measurements in the supercooled state, this non-Arrhenius behavior can be experimentally confirmed in supercooled $Co(hmba)_3[CoBr_4]$ (Figure 7b). Over the entire temperature range measured ($0.9 < T_m/T < 1.08$), the viscosity of $Co(hmba)_3[CoBr_4]$ can be well described ($r^2 > 0.99$) by the Vogel–Fulcher–Tammann (VFT) equation

$$\log \eta(T) = \log \eta_\infty + \frac{B}{T - T_0}$$

where η_∞ is the infinite temperature asymptote, B is a temperature-independent constant, and T_0 is the hypothesized ideal glass transition temperature at which the entropies of the glass and the crystal become identical. The VFT model for $Co(hmba)_3[CoBr_4]$ predicts a T_g of 20 °C when extrapolated to $\eta = 10^{12}$ Pa·s (rheological definition of the glass transition), which is in excellent agreement with DSC determined T_g of 21 °C upon cooling. However, the VFT model predicts a viscosity divergence at T_0, which has not been shown to occur experimentally.[35] As such, we also fit the viscosity data of $Co(hmba)_3[CoBr_4]$ with the Mauro–Yue–Ellison–Gupta–Allan (MYEGA) equation

$$\log \eta(T) = \log \eta_\infty + \frac{K}{T} \exp\left(\frac{C}{T}\right)$$

where K and C are temperature-independent constants. This produces a similar high-quality fit ($r^2 > 0.99$) as the VFT equation but yields a slightly lower predicted T_g of 6 °C (Figure S45). These differences are likely due to uncertainties in extrapolating from a relatively narrow range of experimental data, and viscosity data over a wider range of temperatures should provide more insight into the dynamics of supercooled metal–bis(acetamide) liquids.

CONCLUSION

The foregoing results demonstrate strategies to lower the melting temperatures of two- and three-dimensional metal–organic networks through a series of metal–bis(acetamide) compounds that undergo reversible melting transitions from 106 to 262 °C. The low-melting temperatures of these compounds are attributed to weak metal–amide coordination bonds, conformationally flexible bridging ligands, and weak electrostatic interactions. Moreover, we have elucidated the specific structural and chemical features that drive differences in melting thermodynamics within these series of compounds. For instance, we have shown that entropy and enthalpy of fusion are decoupled in these systems, with differences in ΔH_{fus} among isoreticular metal–bis(acetamide) networks largely dictated by metal–ligand bond strength and ΔS_{fus} dependent on the degree to which residual motion is restricted in the solid state. This leads to unexpected situations in which stronger interactions in the solid state can be associated with either melting temperature increases or decreases depending on the nature of entropic effects and highlights the important role that entropy, in addition to enthalpy, plays in determining the melting temperatures of metal–organic networks. Additionally, EXAFS and PDF analyses demonstrate coordination between metal centers and bridging organic ligands in the liquid phase of $Co(bba)_3[CoCl_4]$ and extended-range structural correlations that persist to at least 80 Å, collectively demonstrating the network-forming nature of this liquid.

As dynamic systems with short-range order, long-range disorder, and a combination of solid-like and gas-like behaviors, liquids have long provided important fundamental insights relevant to many areas of science.[36] Owing to their tunable and predictable interactions, coordination network-forming liquids provide a platform to establish new structure–property relationships and realize functionalities not found in conventional liquids. The relationships we have identified between metal–organic network structure, composition, and melting thermodynamics will support future efforts to synthesize new classes of metal–organic frameworks that can be melted into stable and tunable network-forming liquids. For instance, we are applying similar strategies to achieve low melting temperatures in frameworks with more rigid bridging ligands that better fix the relative orientation and arrangement of metal-binding groups and with noncoordinating anions covalently bound to organic bridging ligands bearing neutral donor groups. Both approaches provide opportunities to achieve predictable control over the local structure of liquids and, consequently, the spatiotemporal fluctuations that determine the size, shape, and lifetime of transient voids within them.

ASSOCIATED CONTENT

Supporting Information

The Supporting Information is available free of charge at https://pubs.acs.org/doi/10.1021/jacs.0c11718.

Additional experimental details, powder X-ray diffraction data, EXAFS data, total X-ray scattering data, pair distribution function analysis, calorimetry data, rheological data analysis, and crystallographic information (PDF)

Accession Codes

CCDC 2055036–2055050 contain the supplementary crystallographic data for this paper. These data can be obtained free of charge via www.ccdc.cam.ac.uk/data_request/cif, or by emailing data_request@ccdc.cam.ac.uk, or by contacting The Cambridge Crystallographic Data Centre, 12 Union Road, Cambridge CB2 1EZ, UK; fax: +44 1223 336033.

AUTHOR INFORMATION

Corresponding Author

Jarad A. Mason − *Department of Chemistry & Chemical Biology, Harvard University, Cambridge, Massachusetts 02138, United States;* orcid.org/0000-0003-0328-7775; Email: mason@chemistry.harvard.edu

https://dx.doi.org/10.1021/jacs.0c11718
J. Am. Chem. Soc. XXXX, XXX, XXX−XXX

Authors

Mengtan Liu − *Department of Chemistry & Chemical Biology, Harvard University, Cambridge, Massachusetts 02138, United States*

Ryan D. McGillicuddy − *Department of Chemistry & Chemical Biology, Harvard University, Cambridge, Massachusetts 02138, United States*

Hung Vuong − *Department of Chemistry, Columbia University, New York 10027, United States*

Songsheng Tao − *Department of Applied Physics and Applied Mathematics, Columbia University, New York 10027, United States*

Adam H. Slavney − *Department of Chemistry & Chemical Biology, Harvard University, Cambridge, Massachusetts 02138, United States*

Miguel I. Gonzalez − *Department of Chemistry & Chemical Biology, Harvard University, Cambridge, Massachusetts 02138, United States*

Simon J. L. Billinge − *Department of Applied Physics and Applied Mathematics, Columbia University, New York 10027, United States; Condensed Matter Physics and Materials Science Department, Brookhaven National Laboratory, Upton, New York 11973, United States;* orcid.org/0000-0002-9734-4998

Complete contact information is available at: https://pubs.acs.org/10.1021/jacs.0c11718

Notes

The authors declare no competing financial interest.

■ ACKNOWLEDGMENTS

This research was partially supported by the Arnold and Mabel Beckman Foundation through a Beckman Young Investigator grant awarded to J.A.M. and Beckman Postdoctoral Fellowships to M.I.G. and A.H.S. Synthesis, crystallography, thermal characterization, and EXAFS experiments were supported by the Office of Naval Research under Award No. N00014-19-1-2148. Studies of metal−bis(acetamide) glass formation were supported by the U.S. Department of Energy (DoE) under Award No. DE-SC0021145. The PDF work was supported by the NSF MRSEC program through Columbia in the Center for Precision Assembly of Quantum Materials (PAQM) (DMR-2011738). We thank Dr. Shao-Liang Zheng for assistance with crystallography experiments and data analysis. We thank Dr. Sungsik Lee for assistance with EXAFS experiments and data analysis. EXAFS measurements were conducted on beamline 12-BM at the Advanced Photon Source, a DoE Office of Science User Facility operated for the DoE Office of Science by Argonne National Laboratory under Contract No. DE-AC02-06CH11357. We thank Dr. Maxwell Terban for assistance with PDF data analysis. X-ray PDF measurements were conducted on beamline 28-ID-2 of the National Synchrotron Light Source II, a U.S. Department of Energy (DOE) Office of Science User Facility operated for the DOE Office of Science by Brookhaven National Laboratory under Contract No. DE-SC0012704.

■ REFERENCES

(1) (a) Agarwal, M.; Chakravarty, C. Relationship between Structure, Entropy, and Mobility in Network-Forming Ionic Melts. *Phys. Rev. E* **2009**, *79*, No. 030202. (b) Agarwal, M.; Ganguly, A.; Chakravarty, C. Transport Properties of Tetrahedral, Network-Forming Ionic Melts. *J. Phys. Chem. B* **2009**, *113*, 15284−15292. (c) Wilson, M.; Salmon, S. P. Network Topology and the Fragility of Tetrahedral Glass-Forming Liquids. *Phys. Rev. Lett.* **2009**, *103*, 157801.

(2) (a) Turbull, D.; Bagley, B. G. Transitions in Viscous Liquids and Glasses. In *Changes of State*; Hanny, N. B., Ed.; Springer: Boston, 1975; pp 513−554. (b) Roberts, C. J.; Debenedetti, P. G. Polyamorphism and Density Anomalies in Network-Forming Fluids: Zeroth- and First-Order Approximations. *J. Chem. Phys.* **1996**, *105*, 658−672. (c) Roberts, C. J.; Panagiotopoulos, A. Z.; Debenedetti, P. G. Liquid−Liquid Immiscibility in Pure Fluids: Polymorphism in Simulations of a Network-Forming Fluid. *Phys. Rev. Lett.* **1996**, *77*, 4386−4389. (d) Poole, P. H.; Grande, T.; Angell, C. A.; McMillan, P. F. Polyamorphic Phase Transitions in Liquids and Glasses. *Science* **1997**, *275*, 322−323. (e) Yarger, J. L.; Angell, C. A.; Borick, S. S.; Wolf, G. H. Polyamorphic Transitions in Network-Forming Liquids and Glasses. In *Supercooled Liquids*; Fourkas, J. T., Kivelson, D., Mohanty, U., Nelson, K. A., Eds.; ACS Symposium Series 676; American Chemical Society: Washington, DC, 1997; pp 214−223. (f) Wilson, M. Structure and Dynamics in Network-Forming Materials. *J. Phys.: Condens. Matter* **2016**, *28*, 503001−503031.

(3) (a) Yaghi, O. M.; O'Keeffe, M.; Ockwing, N. W.; Chae, H. K.; Eddaoudi, M. Reticular Synthesis and the Design of New Materials. *Nature* **2003**, *423*, 705−714. (b) Kitagawa, S.; Kitaura, R.; Noro, S. Functional Porous Coordination Polymers. *Angew. Chem., Int. Ed.* **2004**, *43*, 2334−2375. (c) Férey, G. Hybrid Porous Solids: Past, Present, Future. *Chem. Soc. Rev.* **2008**, *37*, 191−214. (d) Yaghi, O. M. Reticular Chemistry: Molecular Precision in Infinite 2D and 3D. *Molecular Frontiers Journal* **2019**, *3*, 1−18.

(4) (a) Gaillac, R.; Pullumbi, P.; Beyer, K. A.; Chapman, K. W.; Keen, D. A.; Bennett, T. D.; Coudert, F. X. Liquid Metal−Organic Frameworks. *Nat. Mater.* **2017**, *16*, 1149−1154. (b) Bennett, T. D.; Horike, S. Liquid, Glass and Amorphous Solid States of Coordination Polymers and Metal−Organic Frameworks. *Nat. Rev. Mater.* **2018**, *3*, 431−440. (c) Gaillac, R.; Pullumbi, P.; Coudert, F.-X. Melting of Zeolitic Imidazolate Frameworks with Different Topologies: Insight from First-Principles Molecular Dynamics. *J. Phys. Chem. C* **2018**, *122*, 6730−6736. (d) Horike, S.; Nagarkar, S. S.; Ogawa, T.; Kitagawa, S. A New Dimension for Coordination Polymers and Metal−Organic Frameworks: Towards Functional Glasses and Liquids. *Angew. Chem., Int. Ed.* **2020**, *59*, 6652−6664.

(5) Moghadam, P. Z.; Li, A.; Wiggin, S. B.; Tao, A.; Maloney, A. G.; Wood, P. A.; Ward, S. C.; Fairen-Jimenez, D. Development of a Cambridge Structural Database Subset: A collection of Metal−Organic Frameworks for Past, Present, and Future. *Chem. Mater.* **2017**, *29*, 2618−2625.

(6) (a) Bennett, T. D.; Tan, J.-C.; Yue, Y.; Baxter, E.; Ducati, C.; Terrill, N. J.; Yeung, H. H. -M.; Zhou, Z.; Chen, W.; Henke, S.; Cheetham, A. K.; Greaves, G. N. Hybrid Glasses from Strong and Fragile Metal−Organic Framework liquids. *Nat. Commun.* **2015**, *6*, 8079. (b) Umeyama, D.; Horike, S.; Inukai, M.; Itakura, T.; Kitagawa, S. Reversible Solid-to-Liquid Phase Transition of Coordination Polymer Crystals. *J. Am. Chem. Soc.* **2015**, *137*, 864−870. (c) Bennett, T. D.; Yue, Y.; Li, P.; Qiao, A.; Tao, H.; Greaves, N. G.; Richards, T.; Lampronti, G. I.; Redfern, S. A. T.; Blanc, F.; Farha, O. K.; Hupp, J. T.; Cheetham, A. K.; Keen, D. A. Melt-Quenched Glasses of Metal−Organic Frameworks. *J. Am. Chem. Soc.* **2016**, *138*, 3484−3492. (d) Zhou, C.; Longley, L.; Krajnc, A.; Smales, G. J.; Qiao, A.; Erucar, I.; Doherty, C. M.; Thornton, A. W.; Hill, A. J.; Ashling, C. W.; Qazvini, O. T.; Lee, S. J.; Chater, P. A.; Terrill, N. J.; Smith, A. J.; Yue, Y.; Mail, G.; Keen, D. A.; Telfer, S. G.; Bennett, T. D. Metal−Organic Frameworks Glasses with Permanent Accessible Porosity. *Nat. Commun.* **2018**, *9*, 5042. (e) Frentzel-Beyme, L.; Kloß, M.; Kolodzeiski, P.; Pallach, R.; Henke, S. Meltable Mixed-Linker Zeolitic Imidazolate Frameworks and Their Microporous Glasses: From Melting Point Engineering to Selective Hydrocarbon Sorption. *J. Am. Chem. Soc.* **2019**, *141*, 12362−12371. (f) Kimata, H.; Mochida, T. *Chem. Eur. J.*, Crystal Structures and Melting Behaviors of 2D and 3D Anionic Coordination Polymers Containing Organometallic Ionic Liquid Components. *Chem. - Eur. J.* **2019**, *25*, 10111−10117.

(g) Nagarkar, S. S.; Kurasho, H.; Duong, N. T.; Nishiyama, Y.; Kitagawa, S.; Horike, S. Crystal Melting and Glass Formation in Copper Thiocyanate Based Coordination Polymers. *Chem. Commun.* **2019**, *55*, 5455−5458. (h) Widmer, R. N.; Lampronti, G. I.; Anzellini, S.; Gaillac, R.; Farsang, S.; Zhou, C.; Belenguer, A. M.; Palmer, H.; Kleppe, A. K.; Wharmby, M. T.; Redfern, S. A.; Coudert, F.-X.; MacLeod, S. G.; Bennett, T. Pressure Promoted Low-Temperature Melting of Metal−Organic Frameworks. *Nat. Mater.* **2019**, *18*, 370−376. (i) Das, C.; Ogawa, T.; Horike, S. Stable Melt Formation of 2D Nitrile-Based Coordination Polymer and Hierarchical Crystal−Glass Structuring. *Chem. Commun.* **2020**, *56*, 8980−8983. (j) Hou, J.; Gómez, M. L. R.; Krajnc, A.; McCaul, A.; Li, S.; Bumstead, A. M.; Sapnik, A. F.; Deng, Z.; Lin, R.; Chater, P. A.; Keeble, D. S.; Keen, D. A.; Appadoo, D.; Chan, B.; Vicki, Chen.; Mali, G.; Bennett, T. D. Halogenated Metal−Organic Framework Glasses and Liquids. *J. Am. Chem. Soc.* **2020**, *142*, 3880−3890. (k) Das, C.; Horike, S. Crystal Melting and Vitrification Behaviors of the Three-Dimensional Nitrile-Based Metal−Organic Framework. *Faraday Discuss.*, **2021**, DOI: 10.1039/D0FD00003E.

(7) A brief comment on semantics: many terms, including "metal−organic frameworks" (MOFs), "coordination polymers", and "coordination network solids", are currently used to describe solid-state structures composed of inorganic units linked by bridging organic ligands through coordination bonds to form extended networks. Although "metal−organic framework liquids" has recently been used to refer to the liquid phases of ZIF compounds, we believe that the more general descriptors "coordination network-forming liquid" or "metal−organic network-forming liquid" better capture the interconnectedness of inorganic units and bridging organic ligands in the liquid state and the resulting structural correlations that are imparted by the directional nature of dynamic coordination bonds. Moreover, such terminology is consistent with the long-standing use of "network-forming liquids" in the physical chemistry community to describe liquids, such as H_2O and molten SiO_2, with structural correlations that resemble those of a parent crystalline network and are mediated by other types of directional interactions, such as hydrogen bonding and covalent bonds.

(8) Longley, L.; Collins, S. M.; Li, S.; Smales, G. J.; Erucar, I.; Qiao, A.; Hou, J.; Doherty, C. M.; Thornton, A. W.; Hill, A. J.; Yu, X.; Nicholas, T. J.; Smith, A. J.; Cohen, S. M.; Midgley, P. A.; Keen, D. A.; Telfer, S. G.; Bennett, T. D. Flux Melting of Metal−Organic Frameworks. *Chem. Sci.* **2019**, *10*, 3592−3601.

(9) Mullin, J. B. Single Crystal Growth I: Melt Growth. In *Electronic Materials*; Miller, L. S., Mullin, J. B., Eds.; Springer: Boston, 1991; pp 111−126.

(10) (a) Bennett, T. D.; Cheetham, A. K. Amorphous Metal−Organic Frameworks. *Acc. Chem. Res.* **2014**, *47*, 1555−1562. (b) Chen, W.; Horike, S.; Umeyama, D.; Ogiwara, N.; Itakura, T.; Tassel, C.; Goto, Y.; Kageyama, H.; Kitagawa, S. Glass Formation of a Coordination Polymer Crystal for Enhanced Proton Conductivity and Material Flexibility. *Angew. Chem., Int. Ed.* **2016**, *55*, 5195−5200. (c) Zhao, Y.; Lee, S.-Y.; Becknell, N.; Yaghi, O. M.; Angell, C. A. Nanoprous Transparent MOF Glasses with Accessible Internal Surface. *J. Am. Chem. Soc.* **2016**, *138*, 10818−10821. (d) Qiao, A.; Bennett, T. D.; Tao, h.; Krajnc, A.; Mali, G.; Doherty, C. M.; Thornton, A. W.; Mauro, J. C.; Greaves, G. N.; Yue, Y. A Metal−Organic Framework with Ultrahigh Glass-forming Ability. *Sci. Adv.* **2018**, *4*, eaao6827. (e) Inukai, M.; Nishiyama, Y.; Honjo, K.; Das, C.; Kitagawa, S.; Horike, S. Glass-Phase Coordination Polymer Displaying Proton Conductivity and Guest-Accessible Porosity. *Chem. Commun.* **2019**, *55*, 8528−8531.

(11) (a) Earle, M. J.; Seddon, K. R. Ionic Liquids. Green Solvents for the Future. *Pure Appl. Chem.* **2000**, *72*, 1391−1398. (b) Dean, P. M.; Turanjanin, J.; Yoshizawa-Fujita, M.; MacFarlane, D. R.; Scott, J. L. Exploring an Anti-Crystal Engineering Approach to the Preparation of Pharmaceutically Active Ionic Liquids. *Cryst. Growth Des.* **2009**, *9*, 1137−1145. (c) Welton, T.; Hallett, J. P. Room-Temperature Ionic Liquids: Solvents for Synthesis and Catalysis. 2. *Chem. Rev.* **2011**, *111*, 3508−3576.

(12) Butler, K. T.; Walsh, A.; Cheetham, A. K.; Kieslich, G. Organised Chaos: Entropy in Hybrid Inorganic−Organic Systems and Other Materials. *Chem. Sci.* **2016**, *7*, 6316−6324.

(13) (a) Dannenfelser, R.-M.; Yalkowsky, S. H. Estimation of Entropy of Melting from Molecular Structure: A Non-Group Contribution Method. *Ind. Eng. Chem. Res.* **1996**, *35*, 1483−1486. (b) Gilbert, A. S. Entropy−Enthalpy Compensation in the Fusion or Organic Molecules: Implications for Walden's Rule and Molecular Freedom in Liquid State. *Thermochim. Acta* **1999**, *339*, 131−142. (c) Wei, J. Molecular Symmetry, Rotational Entropy, and Elevated Melting Points. *Ind. Eng. Chem. Res.* **1999**, *38*, 5019−5027.

(14) (a) Goodgame, D. M. L.; Grachvogel, D. A.; Hussain, I.; White, A. J. P.; Williams, D. J. Formation of Polymeric Network Arrays by Complexes of Manganese(II) or Cobalt (II) with Alkane Chain Linked Bis(amide) Ligands of Biological Relevance. *Inorg. Chem.* **1999**, *38*, 2057−2063. (b) Chatterton, N. P.; Goodgame, D. M. L.; Grachvogel, D. A.; Hussain, I.; White, A. J. P.; Williams, D. J. Influence of the Counteranion on the Formation of Polymeric Networks by Metal Complexes of Hexamethylenebis(acetamide). *Inorg. Chem.* **2001**, *40*, 312−317. (c) Alexandru, M.-G.; Jitaru, I.; Madalan, A. M.; Andruh, M. Aggregation of Two Different Coordination Polymers by Reacting Zinc Nitrate and Cadmium Chloride with N, N'−Ethylenebisacetamide. *J. Coord. Chem.* **2011**, *64*, 3333−3341.

(15) Nimmermark, A.; Öhrström, L.; Reedijk, J. Metal-Ligand Bond Lengths and Strengths: Are They Correlated? A Detailed CSD Analysis. *Z. Kristallogr. - Cryst. Mater.* **2013**, *228*, 311−317.

(16) Ryde, U. A Fundamental View of Enthalpy−Entropy Compensation. *MedChemComm* **2014**, *5*, 1324−1336.

(17) (a) Irving, H.; Williams, R. J. P. The Stability of Transition-metal Complexes. *J. Chem. Soc.* **1953**, 3192−3210. (b) Helm, L.; Merbach, A. E. Water Exchange on Metal Ions: Experiments and Simulations. *Coord. Chem. Rev.* **1999**, *187*, 151−181.

(18) McGillicuddy, R. D.; Thapa, S.; Wenny, M. B.; Gonzalez, M. I.; Mason, J. A. Metal−Organic Phase-Change Materials for Thermal Energy Storage. *J. Am. Chem. Soc.* **2020**, *142*, 19170−19180.

(19) (a) Williams, D. H.; O'Brien, D. P.; Bardsley, B. Enthalpy/Entropy Compensation as a Competition between Dynamics and Bonding: The Relevance to Melting of Crystals and Biological Aggregates. *J. Am. Chem. Soc.* **2001**, *123*, 737−738. (b) Ventolà, L.; Cuevas-Diarte, M. A.; Ramírez, M.; Oonk, H. A. J.; Mondieig, D.; Negrier, Ph. Melting Behavior in the n-alkanol Family, Enthalpy−Entropy Compensation. *Phys. Chem. Chem. Phys.* **2004**, *6*, 1786−1791.

(20) (a) Jeffrey, G.; An, A. *Introduction to Hydrogen Bonding*; Oxford University Press: Oxford, 1997. (b) Steiner, T. The Hydrogen Bonds in the Solid State. *Angew. Chem., Int. Ed.* **2002**, *41*, 48−76.

(21) Lambert, F. L. Configurational Entropy Revisited. *J. Chem. Educ.* **2007**, *84*, 1548−1550.

(22) (a) Massa, W. *Crystal Structure Determination*; Springer: Wiesbaden, 2015. (b) Neuburger, M. Disorder in Crystal Structures: New Approaches in Finding the Best Model. Ph.D. Dissertation, University of Basel, Basel, Switzerland, 2012.

(23) The rotational entropy difference is estimated by $\Delta S_{fus}^{rot} = R \ln \sigma$, where R is the ideal gas constant and σ is the external rotational symmetry number (σ = 12 $[MCl_4]^{2-}$and σ = 100 for Cl^- and Br^-).

(24) (a) Rosenfeld, Y. Relation Between the Transport Coefficients and the Internal Entropy of Simple Systems. *Phys. Rev. A: At., Mol., Opt. Phys.* **1977**, *15*, 2545−2549. (b) Sharma, R.; Chakraborty, S. N.; Chakravarty, C. Entropy, Diffusivity, and Structural Order in Liquids with Waterlike Anomalies. *J. Chem. Phys.* **2006**, *125*, 204501. (c) Chakravarty, C.; Nayar, D. Water and Water-like Liquids: Relationships between Structure, Entropy and Mobility. *Phys. Chem. Chem. Phys.* **2013**, *15*, 14162−14177.

(25) Gould, S. L.; Tranchemontagne, D.; Yaghi, O. M.; Garcia-Garibay, M. A. Amphidynamic Character of Crystalline MOF-5: Rotational Dynamics of Terephthalate Phenylenes in a Free-Volume, Sterically Hindered Environment. *J. Am. Chem. Soc.* **2008**, *130*, 3246−3237.

https://dx.doi.org/10.1021/jacs.0c11718
J. Am. Chem. Soc. XXXX, XXX, XXX−XXX

(26) (a) Egami, T.; Billinge, S. J. L. *Underneath the Bragg Peaks: Structural Analysis of Complex Materials*, 2nd ed.; Elsevier: Amsterdam, 2012. (b) Juhás, P.; Davis, T.; Farrow, C. L.; Billinge, S. J. L. PDFgetX3: A Rapid and Highly Automatable Program for Processing Powder Diffraction Data into Total Scattering Pair Distribution Functions. *J. Appl. Crystallogr.* **2013**, *46*, 560−566.
(27) (a) Thorpe, M. F. Rigidity Percolation. In *Physics of Disordered Materials*; Alder, D., Fritzsche, H., Ovshinsky, S. R., Eds; Springer: Boston, 1985; pp 55−61. (b) Phillips, J. C.; Thorpe, M. F. Constraint Theory, Vector Percolation and Glass Formation. *Solid State Commun.* **1985**, *53*, 699−702.
(28) (a) Keblinski, P. Molecular Dynamics Study of Screening in Ionic Fluids. *J. Chem. Phys.* **2000**, *113*, 282−291. (b) Del Pópolo, M. G.; Voth, G. A. On the Structure and Dynamics of Ionic Liquids. *J. Phys. Chem. B* **2004**, *108*, 1744−1752.
(29) (a) Elliott, S. R. Extended-range Order, Interstitial Voids and the First Sharp Diffraction Peak of Network Glasses. *J. Non-Cryst. Solids* **1995**, *182*, 40−48. (b) Salmon, P. S.; Martin, R. A.; Mason, P. E.; Cuello, G. J. Topological versus Chemical Ordering in Network Glasses at Intermediate and Extended Length Scales. *Nature* **2005**, *435*, 75−78.
(30) (a) Tao, H.; Bennett, T. D.; Yue, Y. Melt-Quenched Hybrid Glasses from Metal−Organic Frameworks. *Adv. Mater.* **2017**, *29*, 1601705. (b) Longley, L.; Calahoo, C.; Limbach, R.; Xia, Y.; Tuffnell, J. M.; Sapnik, A. F.; Thorne, M. F.; Keeble, D. S.; Keen, D. A.; Wonderaczek, L.; Bennett, T. D. Metal−Organic Framework and Inorganic Glass Composites. *Nat. Commun.* **2020**, *11*, 5800.
(31) Greaves, G. N.; Sen, S. Inorganic Glasses, Glass-Forming Liquids and Amorphizing Solids. *Adv. Phys.* **2007**, *56*, 1−166.
(32) (a) Turnbull, D. Under What Conditions Can a Glass be Formed? *Contemp. Phys.* **1969**, *10*, 473−488. (b) Baird, J. A.; Santiago-Quinonez, D.; Rinaldi, C.; Taylor, L. S. Role of Viscosity in Influencing the Glass-Forming Ability of Organic Molecules from the Undercooled Melt State. *Pharm. Res.* **2012**, *29*, 271−284.
(33) Abbasi, A.; Saghir, M. Z.; Kawaji, M. Evaluation of the Activation Energy of Viscous Flow for a Binary Mixture in Order to Estimate the Thermodiffusion Coefficient. *J. Non-Equilib. Thermodyn.* **2011**, *36*, 23−40.
(34) (a) Böhmer, R.; Angell, C. A. Local and Global Relaxations in Glass Forming Materials. In *Disorder Effects on Relaxational Processes, Glasses, Polymers, Proteins*; Richert, R., Blumen, A., Eds.; Springer-Verlag: Berlin, 1994; pp 11−54. (b) Mel'cuk, A. I.; Ramos, R. A.; Gould, H.; Klein, W.; Mountain, R. D. Long-Lived Structures in Fragile Glass-Forming Liquids. *Phys. Rev. Lett.* **1995**, *75*, 2522−2525.
(35) (a) Hecksher, T.; Nielsen, A. I.; Olsen, N. B.; Dyre, J. C. Little Evidence for Dynamic Divergences in Ultraviscous Molecular Liquids. *Nat. Phys.* **2008**, *4*, 737−741. (b) Zheng, Q.; Mauro, J. C. Viscosity of Glass-Forming Systems. *J. Am. Ceram. Soc.* **2017**, *100*, 6−25.
(36) (a) Angell, A. Thermodynamics: Liquid Landscape. *Nature* **1998**, *393*, 521−524. (b) Debenedetti, P. G.; Stillinger, F. H. Supercooled Liquids and the Glass Transition. *Nature* **2001**, *410*, 259−267. (c) Chandler, D. From 50 Years Ago, the Birth of Modern Liquid-State Science. *Annu. Rev. Phys. Chem.* **2017**, *68*, 19−38.

https://dx.doi.org/10.1021/jacs.0c11718
J. Am. Chem. Soc. XXXX, XXX, XXX−XXX